

Chapter 6 Global Phase Diagrams in Terms of Pure Component Properties

The phase behaviour of mixtures is governed directly by intermolecular interactions both between similar and dissimilar molecular entities. In normal circumstances for mixtures of molecules of relatively similar size the relative energy of interaction plays the dominant role in determining the type of phase behaviour. Other influences such as molecular shape and size that contribute only indirectly to the intermolecular interactions generally have a minor role. Both the experimental study and calculation of critical points has proved to be an effective way of classifying the phase behaviour of binary mixtures. Different categories of phase behaviour can be assigned depending, for example, on whether the vapour-liquid critical line is continuous or interrupted or whether upper critical solution phenomena are observed. However, our understanding of the phase behaviour of mixtures is confined largely to mixtures containing components of relatively similar shape and size (Chapter 5).

6.1 Global Phase Diagram for the CSvdW Equation of State

As discussed in Chapter 4, the common most phase behaviour of binary mixtures has been successfully classified in the terms of differences in critical lines (van Konynenburg and Scott, 1980; Deiters and Pegg, 1989; Kraska and Deiters, 1992; Yelash and Kraska, 1998; Wang et al 2000; Lamm and Hall, 2001), the focus has been on mixtures of molecules of either similar size or with a small difference in size between the components. More recently, work has been reported on complex systems such as polar substances, ionic systems, polymer solutions or blends (Kraska, 1996; Yelash and Kraska, 1999; Kolafa et al. 1998, 1999; Imre et al. 1999; Polishuk et al. 2000, 2002).

A feature of most previous global phase diagrams is that they involve unlike interaction terms as exemplified by Eqs. (4.16) to (4.21). An exception, which will be discussed below, is the diagram of Kolafa et al. (1998). The use of interaction terms means that it difficult to apply the global phase diagram to real mixtures, because the interaction terms are not directly accessible via experimental means. The global phase diagrams are often strictly valid for a highly idealized situation such as “hard spheres” with a well-defined size difference. In this chapter, we use the CSvdW equation of state and the global phase diagram is different to one in the chapter 5. We take a slightly different approach by generating a global phase diagram in terms of experimentally accessible quantities, such as diagram would be useful for mixtures of real molecules.

6.1.1 Calculation Details

The global phase diagram was determined by calculating the critical properties of binary mixtures (Chapter 3) characterised solely by differences in the critical temperature and volume. The conformal parameters for the mixture or equivalently the mixture equation of state properties were obtained from the one-fluid mixing rule.

In these mixing rules, we employ for the unlike interactions of f_{ij} and h_{ij} , the function (Eq. 3.42) is without the adjustable parameter

$$f_{ij} = \sqrt{f_{ii}f_{jj}} \quad (6.1)$$

and

$$h_{ij} = (h_{11}^{1/3} + h_{22}^{1/3})^3 / 8 \quad (6.2)$$

Importantly, equation (6.1) and (6.2) do not contain any adjustable combining rule parameters.

In this way, we determined the global phase diagram of binary mixtures with varying differences in the critical volume and temperature. This is in contrast to the work for equal size molecules in Chapter 5. The global phase diagram was constructed by varying the strength of the unlike interaction.

6.1.2 The Global Phase Diagram

Calculations were performed for components with different critical temperatures and different critical volumes using the CSvdW equation of state (Chapter 3). The results of the calculations are plotted in Tr - Vr projections of the global phase diagram in Figure 6.1, where $Vr = V_{22}^C / V_{11}^C$ and $Tr = T_{22}^C / T_{11}^C$. V_{11}^C , V_{22}^C , T_{11}^C and T_{22}^C are the critical volumes and temperatures of the two pure components. In contrast to most global phase diagrams (Chapter 4 & 5), the use of Tr and Vr means that the phase diagram is directly linked to experimental quantities.

The global phase diagram (Figure 6.1) has the same general features as reported in Figure 5.1 (in Chapter 5). The bold curves are lines of the double critical end points (DCEP). The vertical solid line which starts from van Laar point to the top of the diagram is a tricritical line (TCP), it separates Types I/V, VI/VII and II/IV behaviour. The dash-dotted line represents the degenerated critical pressure maximum/minimum (dCPM) line, it is the

boundary state of Types II/VI, III/V and III_m/V_m. The critical pressure step points (CPSP) curves are marked with the dashed lines and it separate types V/V_m and III/III_m.

The critical pressure landing point (CPLP) is a cusp of two CPSP curves, and the value is $T_r = 2.901$ and $V_r = 2.14$. The double critical end cusp point (DCECP) is a cusp of two DCEP curves, the coordinates of the DCECP is $T_r = 2.593$ and $V_r = 1.902$. With the exception at Type VIII behaviour (also in Chapter 5), which was not located, all of the major observed phase behaviour types were found from $T_r = 0$ to 3 and $V_r = 1$ to 4. At all values $V_r > 4$ and $T_r > 1$, type I behaviour was found for all values at T_r to the left of the TCP line. To the right of the TCP, only type V behaviour was observed. When $T_r < 1$, only Types I, II, III and III_m behaviour are observed. Type I behaviour exists in the region above the DCEP line, which is close to $T_r = 1$. Type II was observed between two DCEP lines. The range of type III_m is a narrow area, which is between DCEP line and CPSP line. Under the CPSP line, type III behaviour is located.

A considerable diversity of phase behaviour is confined to a relatively small region of the global phase diagram, which is illustrated in greater detail in Figure 6.2. Figure 6.2 identifies regions in which behaviour of Types IV, V_m, VI and VII occur. As discussed in detail in Chapters 4 and 5, the boundary states between these types of behaviour involve a TCP, a critical pressure set point (CPSP), a critical pressure landing point (CPLP) and a degenerate critical pressure maximum or minimum (dCPM). The transition between different phase behaviour types via some of these states is illustrated in Figures 6.7 to 6.12.

When $V_r = 1$, Types I, II, III_m or III behaviour can be observed depending on the ratio of critical temperatures of the two components. For $V_r > 1$, there are more types of phenomena. Types IV, VI and VII behaviour are confined to the region of $1.1 < V_r < 2$ and $2.1 < T_r < 2.6$.

The observation of types IV, V_m, VI and VII behaviour is significant. Most previous work (van Konynenburg and Scott, 1980; Deiters and Pegg, 1989; Kraska and Deiters, 1991; Yelash and Kraska, 1998; Wang et al., 2000; Lamm and Hall, 2001) that has reported these types of behaviour did so in conjunction with combining rule parameters that represented a significant deviation from the Lorentz-Berthelot combining rules. The results presented here indicate that simply changing the relative values of the critical temperatures and volumes is sufficient to observe type VI and VII behaviour. Examples of these calculations are illustrated in the Figures 6.3 to 6.6.

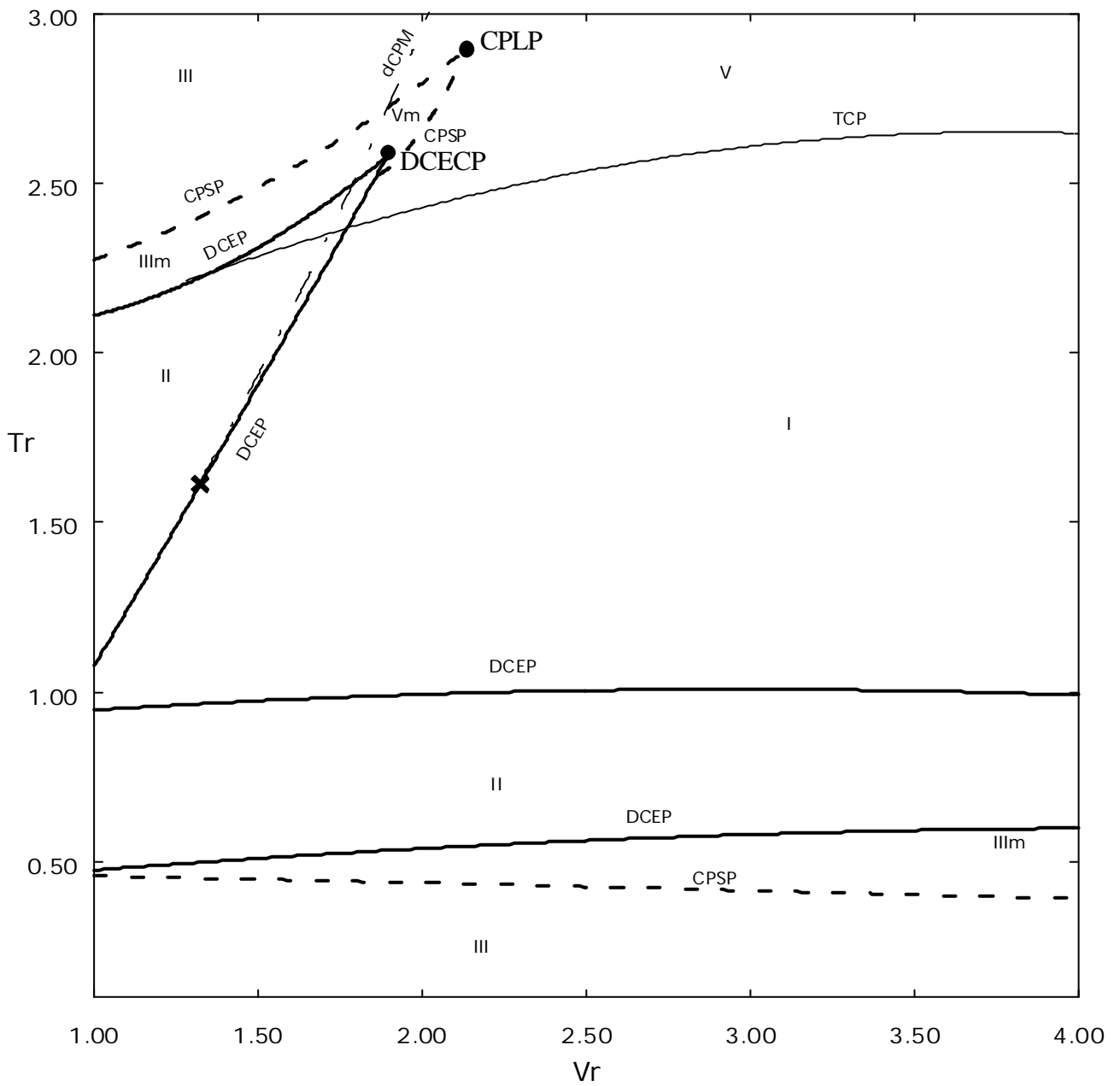


Figure 6.1 Global phase diagram of binary mixtures predicted from the CSvdW equation of state in the absence of adjustable combining rule parameters. The marks ? are double critical end cusp point (DCECP) and the critical pressure landing point (CPLP), and the mark x is van Laar point.

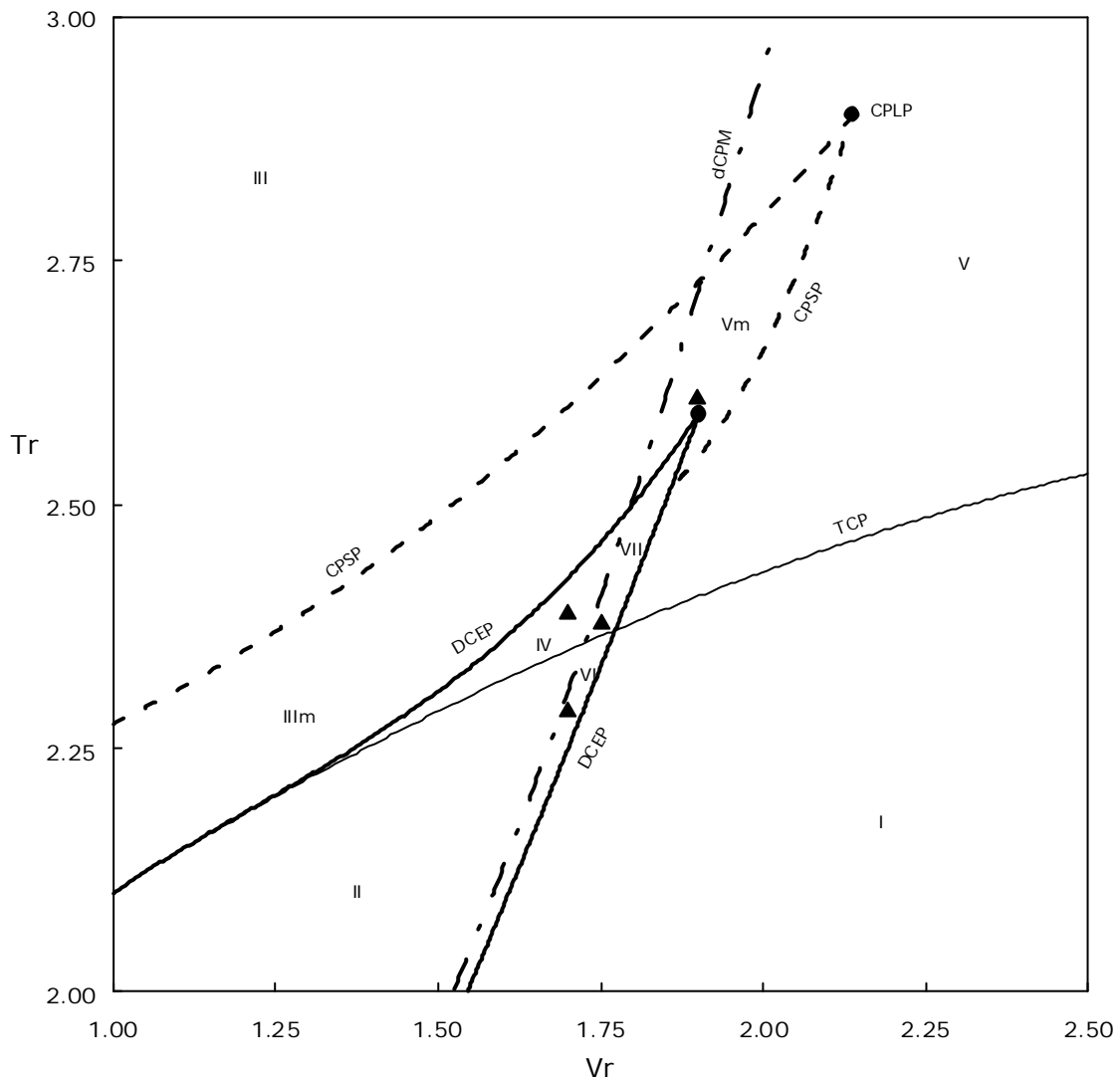


Figure 6.2. Enlargement of the global phase diagram showing regions of types IV, VI, VII and V_m behaviour. The triangles mark the coordinates for calculations illustrated in Figures 6.3-6.6.

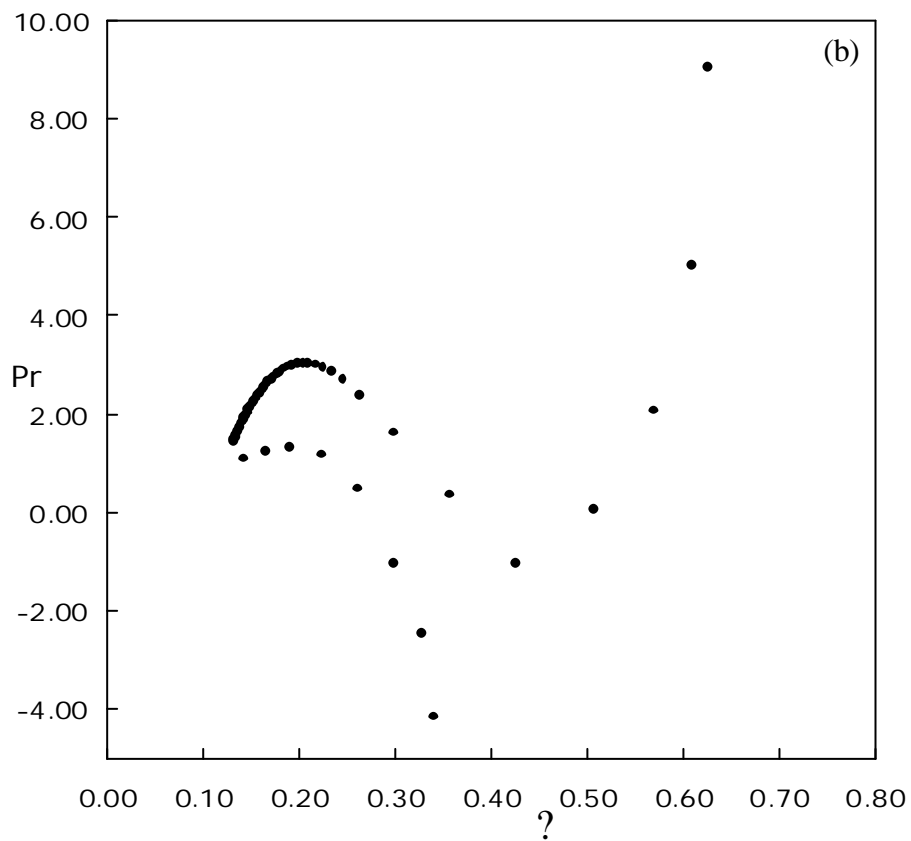
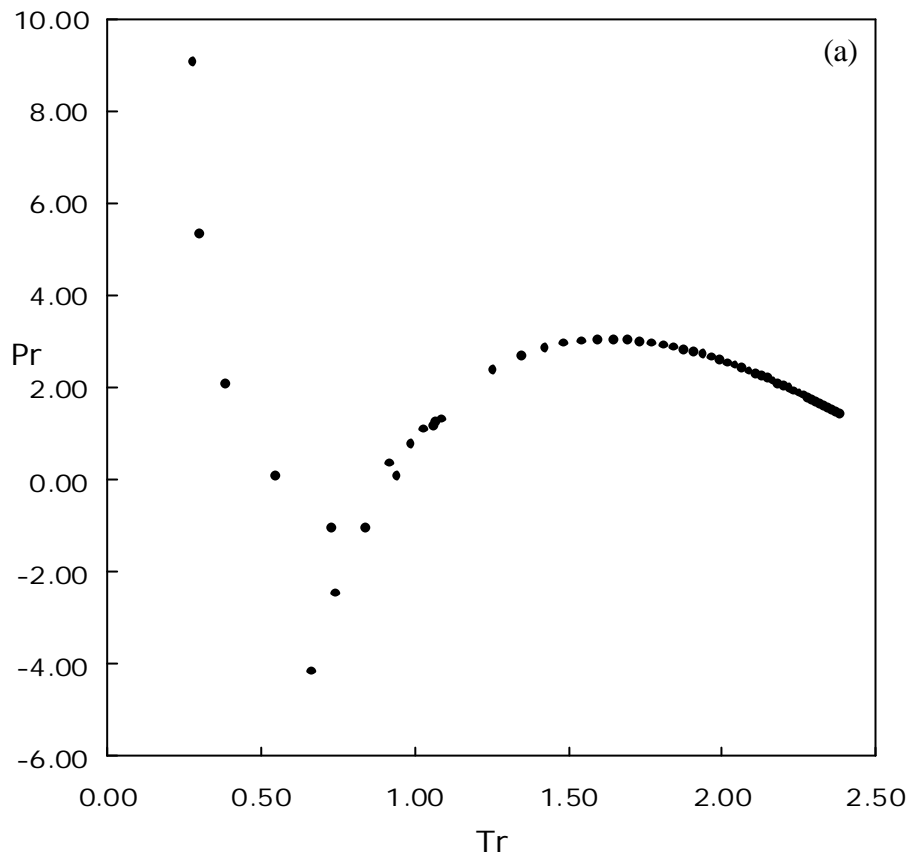


Figure 6.3. The calculated critical properties of a type IV mixture in the (a) pressure-temperature and (b) pressure-packing fraction projections. The location of the mixture is marked in the Figure 6.2 by a filled triangle at $Tr = 2.39$ and $Vr = 1.7$

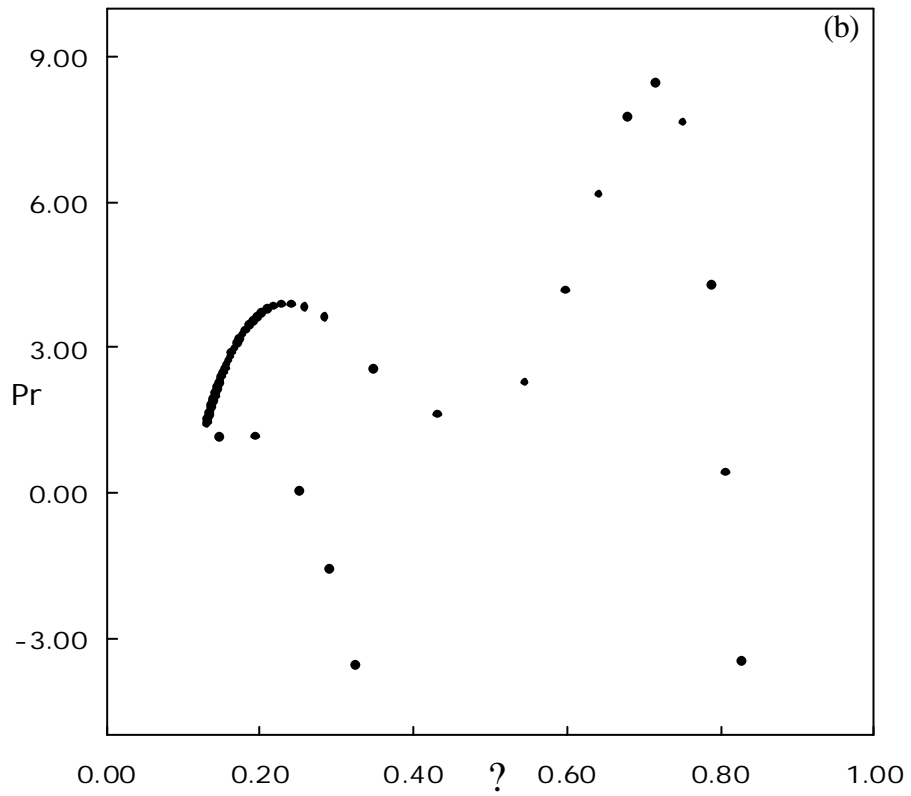
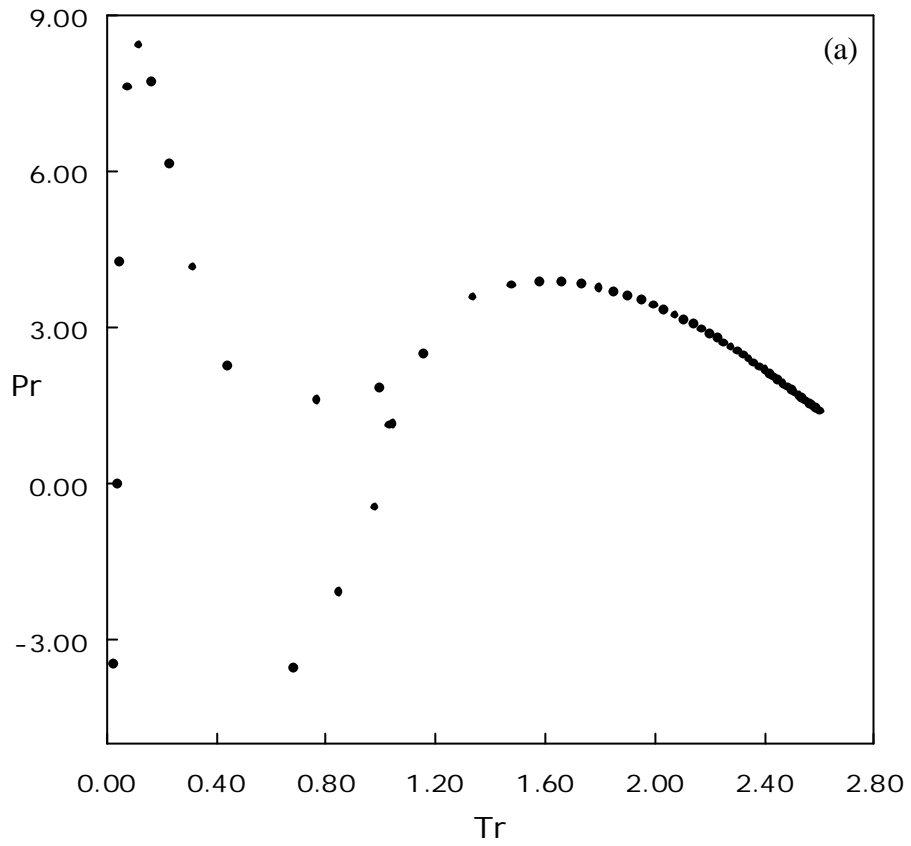


Figure 6.4. The calculated critical properties of a type Vm mixture in the (a) pressure-temperature and (b) pressure-packing fraction projections. The location of the mixture is marked in the Figure 6.2 by a filled triangle at $Tr = 2.61$ and $Vr = 1.9$.

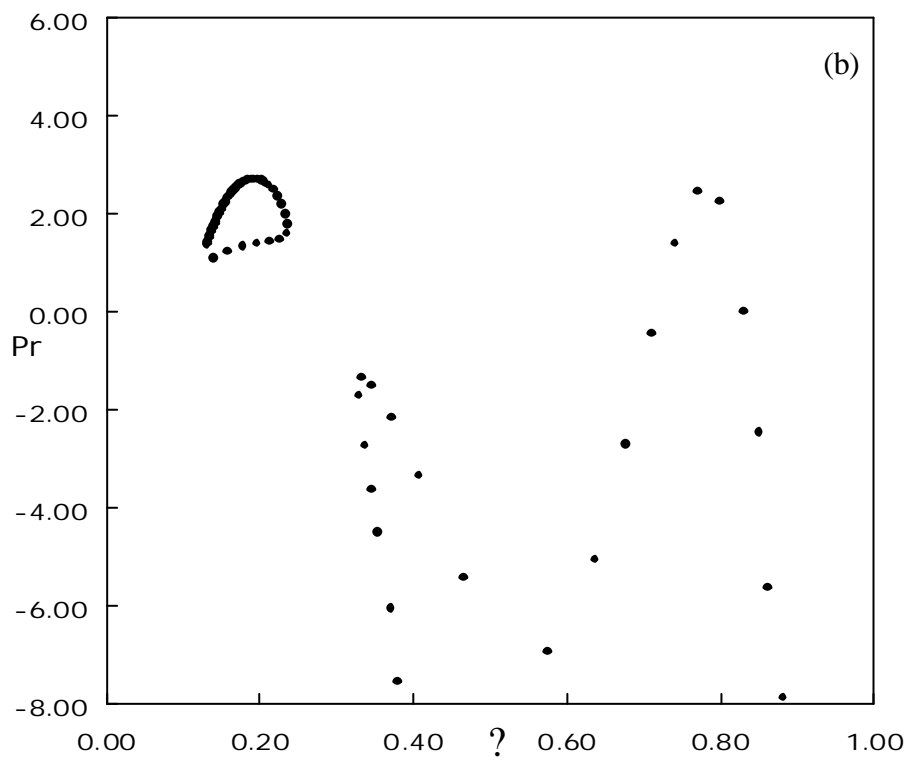
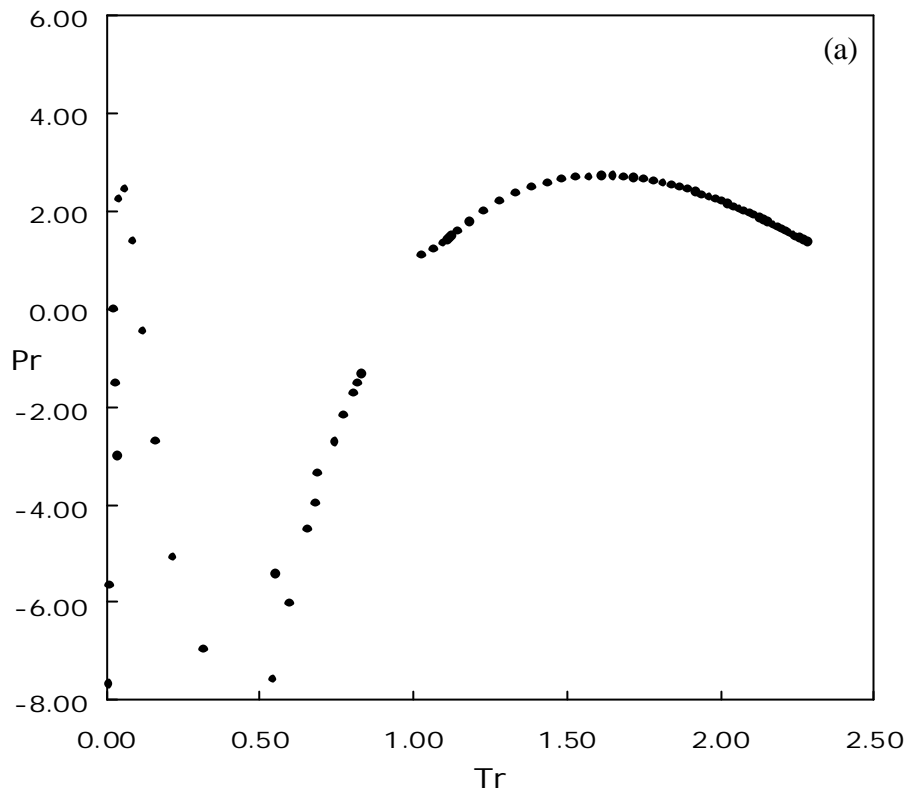


Figure 6.5. The calculated critical properties of a type VI mixture in the (a) pressure-temperature and (b) pressure-packing fraction projections. The location of the mixture is marked in the Figure 6.2 by a filled triangle at $Tr = 2.29$ and $Vr = 1.7$.

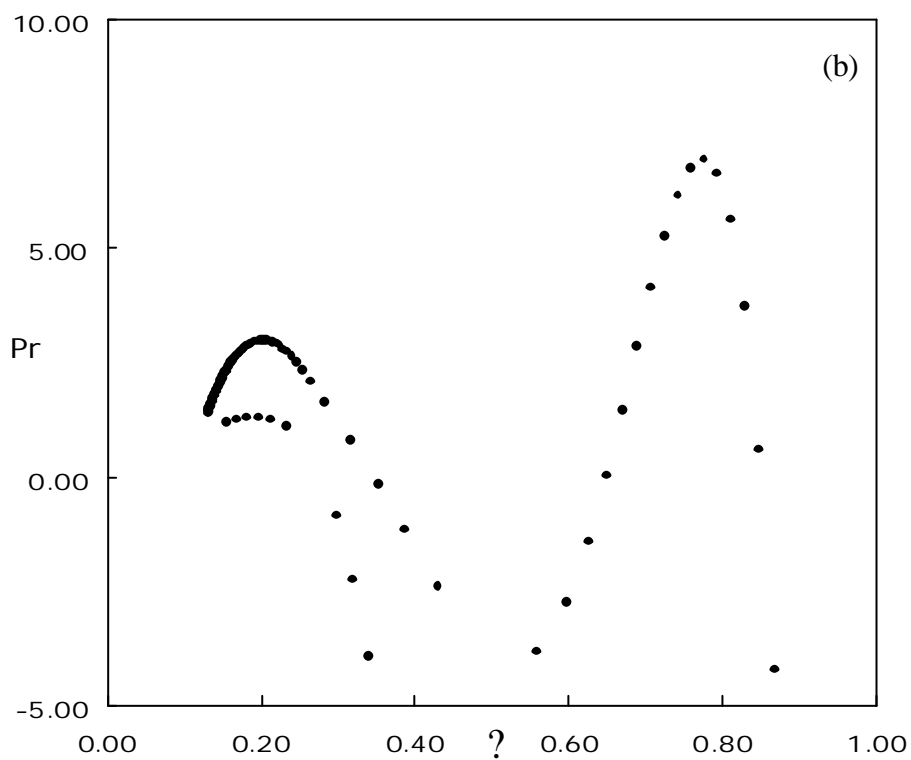
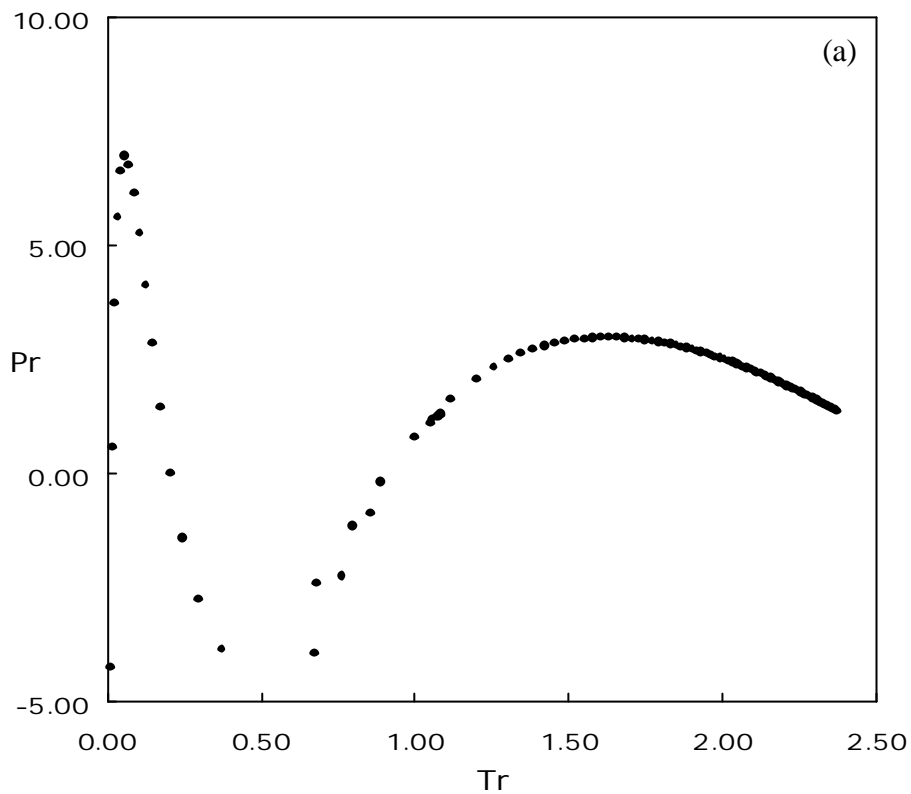


Figure 6.6. The calculated critical properties of a type VII mixture in the (a) pressure-temperature and (b) pressure-packing fraction projections. The location of the mixture is marked in the Figure 6.2 by a filled triangle at $Tr = 2.38$ and $Vr = 1.75$.

The transition between the various types of phase behaviour can be examined in greater detail by taking slices of the global phases diagrams at different values of V_r . The transitions observed when V_r equal to 1.1, 1.3, 1.5, 1.7, 1.9, 3.0 and 4.0, are discussed below.

6.1.3 Phase Type when $V_r = 1.1$

Figure 6.7 illustrates the pressure-temperature projection of calculated critical lines at $V_r = 1.1$ and $Tr = 1.09, 1.12, 2.13, 2.15, 2.29$ and 2.31 , which are close to the boundary state. Figure 6.7a shows the boundary state of types I and II. Normally, there is type VI phenomena between type I and type II, but it is not be observed in some area of global phase diagram. The possible transition between type I and type II, is illustrated in figure 6.7 (a), a DCEP point has a zero Temperature in p - T projection. We have not found the type VI behaviour with CSvdW equation of state in the area of $Tr \in (0.1, 3)$ and $V_r \in (1.0, 4.0)$. In this case of type II, the liquid-liquid critical line has a negative pressure (metastable lines).

In Figure 6.7(b), the transition diagram shows that the vapour-liquid critical line touches the UCEP, which is starting point of the three-phase line. It is a boundary diagram of type III_m and type II. In this case, the diagram of type III_m shows pressure maximum and minimum points on the vapour-liquid critical curves, which start from pure critical point with a high critical temperature (this critical curve emerges with a liquid-liquid critical curve at high pressure), these two point respectively express maximum pressure and minimum pressure. In the first diagram of Figure 6.7c, the two points of maximum pressure and minimum pressure move closer to each other, and emerge together in CPSP point, which is the boundary state of type III_m/III showed in the second diagram of Figure 6.7c.

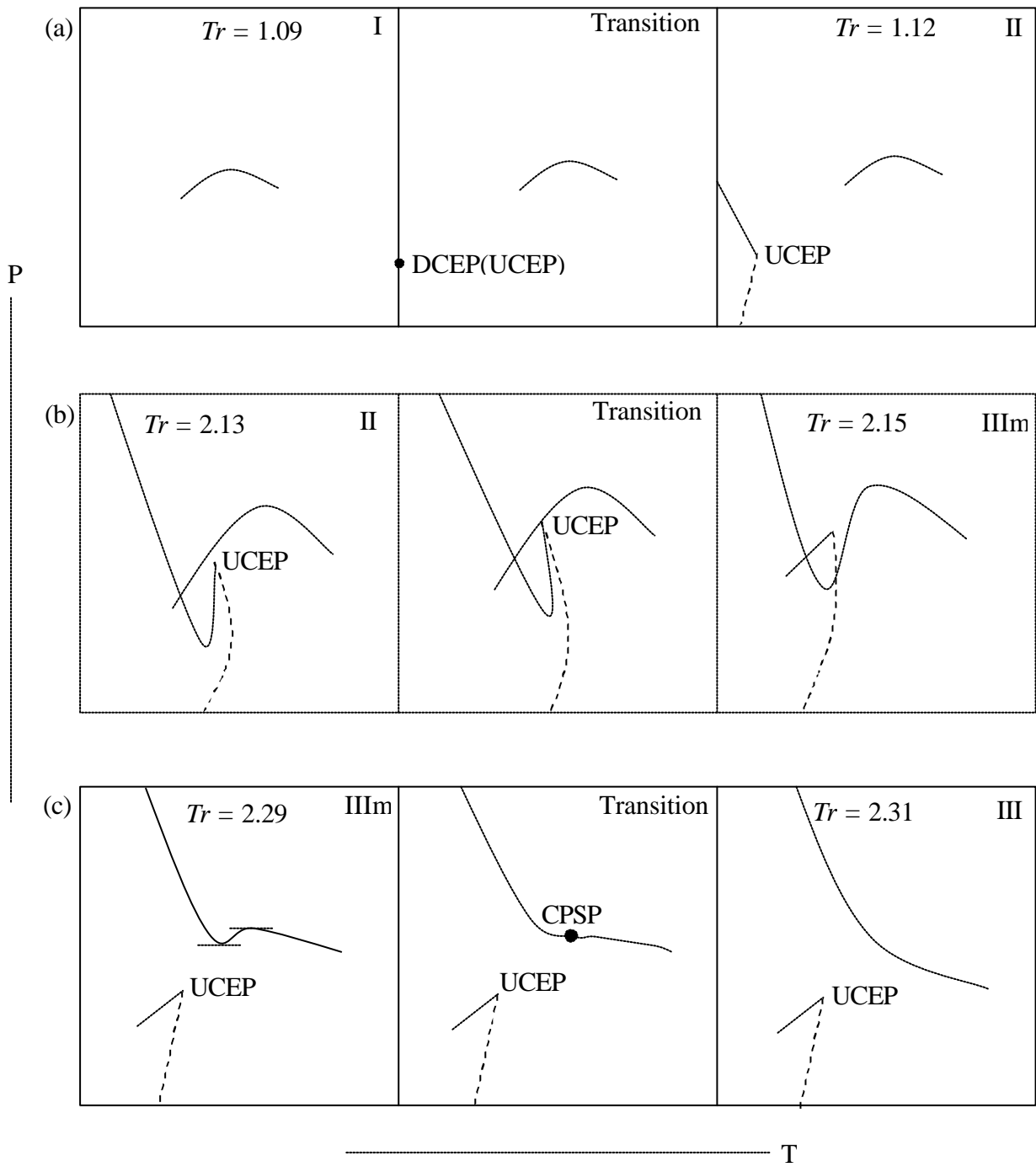


Figure 6.7 The Phase types and boundaries of $Vr = 1.1$. Marks (•) are pure component critical points. The dashed curves represent LLV curves and the full curves are critical curves.

6.1.4 Phase Type when $V_r = 1.3$

For $V_r = 1.3$, type I behaviour occurs between $Tr = 1.0$ and $Tr = 1.592$. Type II behaviour exists in the range of $Tr = 1.593$ and 2.19. DCEP-boundary of type I/II is estimated between Tr being 1.592 and 1.593.

Figure 6.8(a) is the diagram of $Tr = 2.19$. By increasing Tr , the UCEP moves closer to the vapour-liquid critical curve connecting two pure component critical points. This curve becomes discontinuous at TCP. Figure 6.8 (a) shows the transition between type II and type IV behaviour. When the value of Tr is increased, type IV behaviour is found in the range of Tr between 2.21 and 2.23, although this locus is very small, the type IV behaviour is very clear.

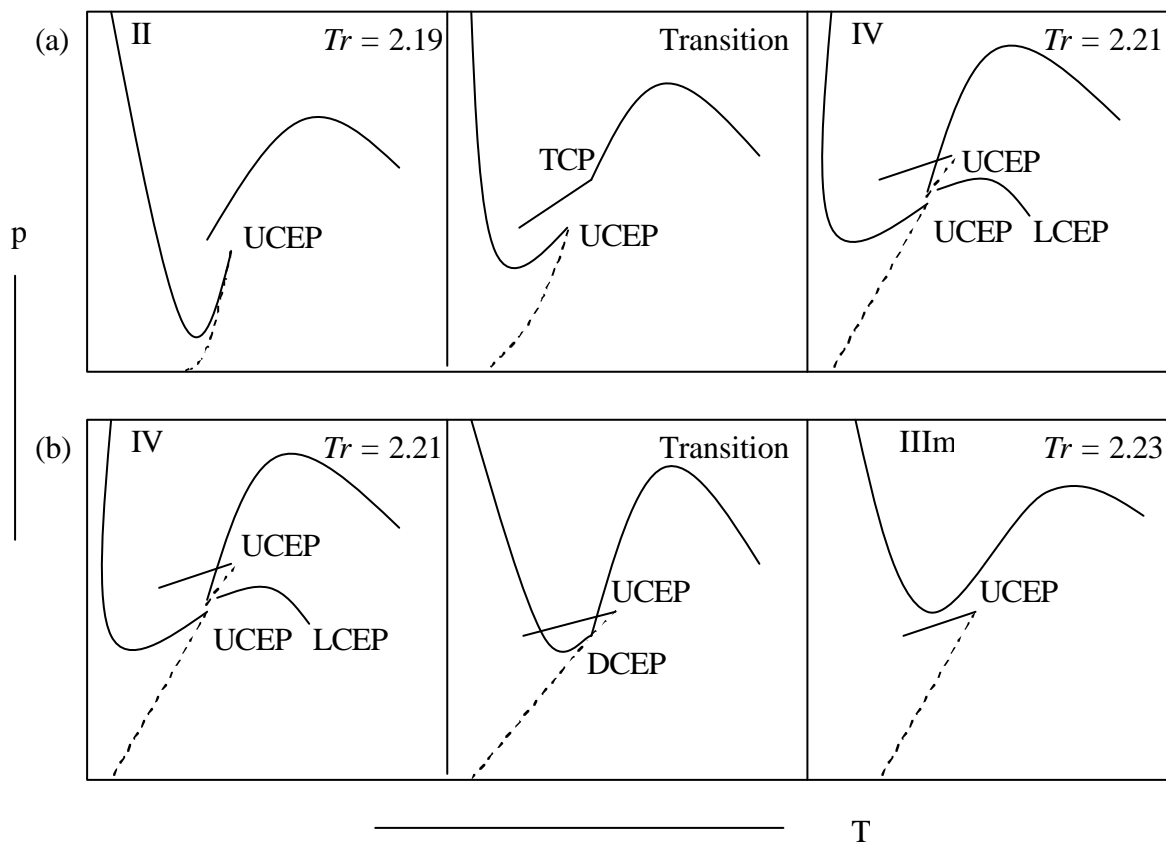


Figure 6.8 The pathway from type II to type IIIm in $V_r = 1.3$. Marks (•) are pure critical points. The dashed curves represent LLV curves and the full curves are critical curves.

Continuing to increase the value of Tr , the LCEP in the type IV of figure 6.8(a) goes away from the UCEP which is the end of vapour-liquid critical curve starting from one pure component critical point, and approaches the UCEP which is the end point of the liquid-liquid critical line. Figure 6.8 (b) shows that type IV behaviour is transformed to type III_m behaviour. The boundary of type IV and type III_m is another DCEP (Figure 6.8(b)). The range of type III_m is $Tr = 2.23$ to $Tr = 2.41$. In this case, there is the same pathway from type III_m to type III are found for $V_r = 1.1$ (Figure 6.7 (c)).

6.1.5 Phase Type when $V_r = 1.5$

For $V_r = 1.5$, type I, VI, II, IV, III_m and III phase behaviour are found. The boundary states, such as TCP is the boundary of types II/IV. DCEP and CPSP, respectively, separate type IV/III_m and type III_m/III. A closed-loop behaviour of type VI, a boundary state DCEP of the type I/VI, and a boundary state dCPM of type VI/II are presented here. The pathway from type I to II is illustrated in Figure 6.9.

In the transition diagram of Figure 6.9(a), the part of the critical line at low temperatures is a DCEP point. The DCEP is the boundary of type I (the first diagram of Figure 6.9(a)) and type VI (the third diagram of Figure 6.9(a)). When Tr is increased to 1.95, the LCEP in the diagram for type VI goes to lower temperature, until it touches the limit of $Tr = 0$. In our calculations, a non zero but very small value for $Tr \rightarrow 0$ has been chosen (The first diagram of Figure 6.9(b)). The transition diagram in Figure 6.9(b) is the boundary state between type VI and type II, and involves a degenerated critical pressure maximum or minimum (dCPM) (Kraska, 1996).

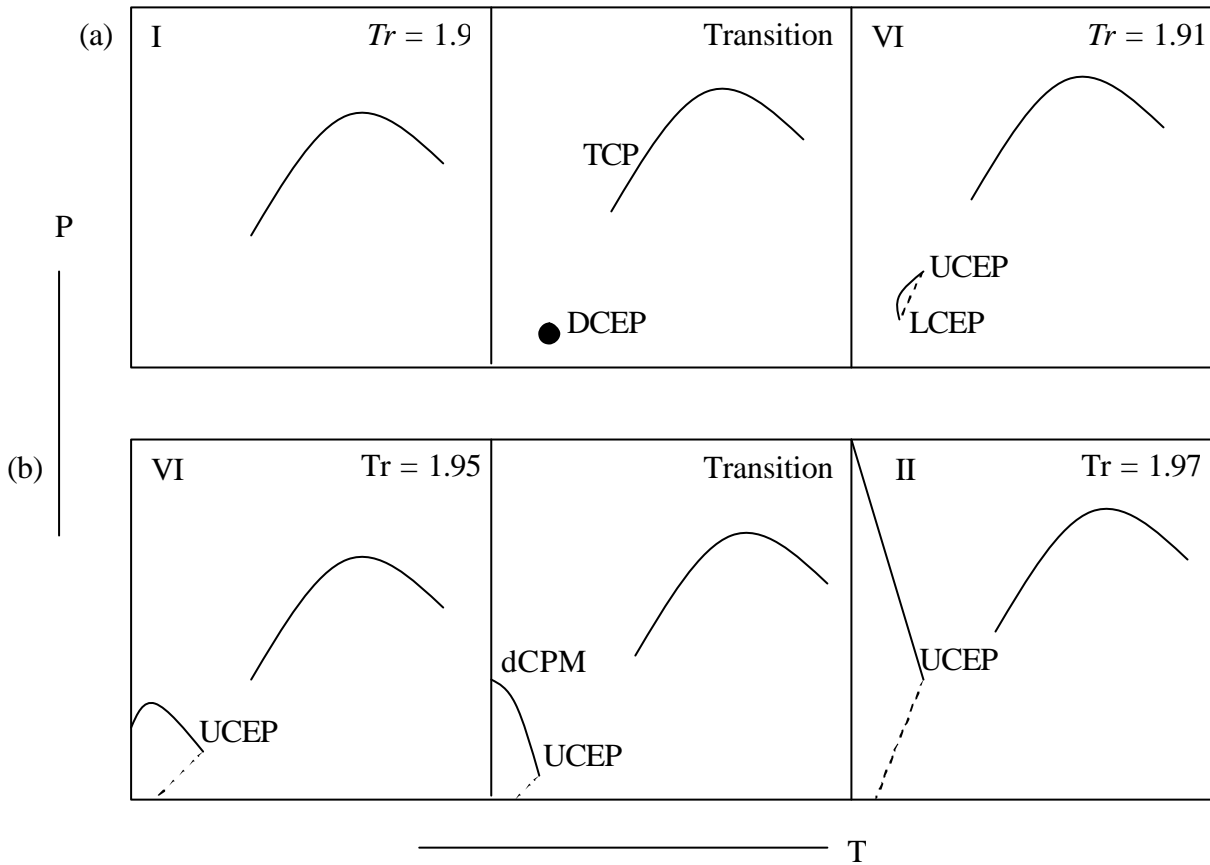


Figure 6.9 The pathway from type I to type II in $Vr = 1.5$. Marks (•) are pure critical points. The dashed curves represent LLV curves and the full curves are critical curves.

6.1.6 Phase Type when $Vr = 1.7$

When $Vr = 1.7$ (Figure 6.10), a considerable diversity of phase behaviour is observed over a relatively small temperature range. Initially, there is a type VI/VII transition via a TCP (Figure 6.10 (a)). Type VI behaviour is in turn transformed to type IV via a dCPM (Figure 6.10 (b)).

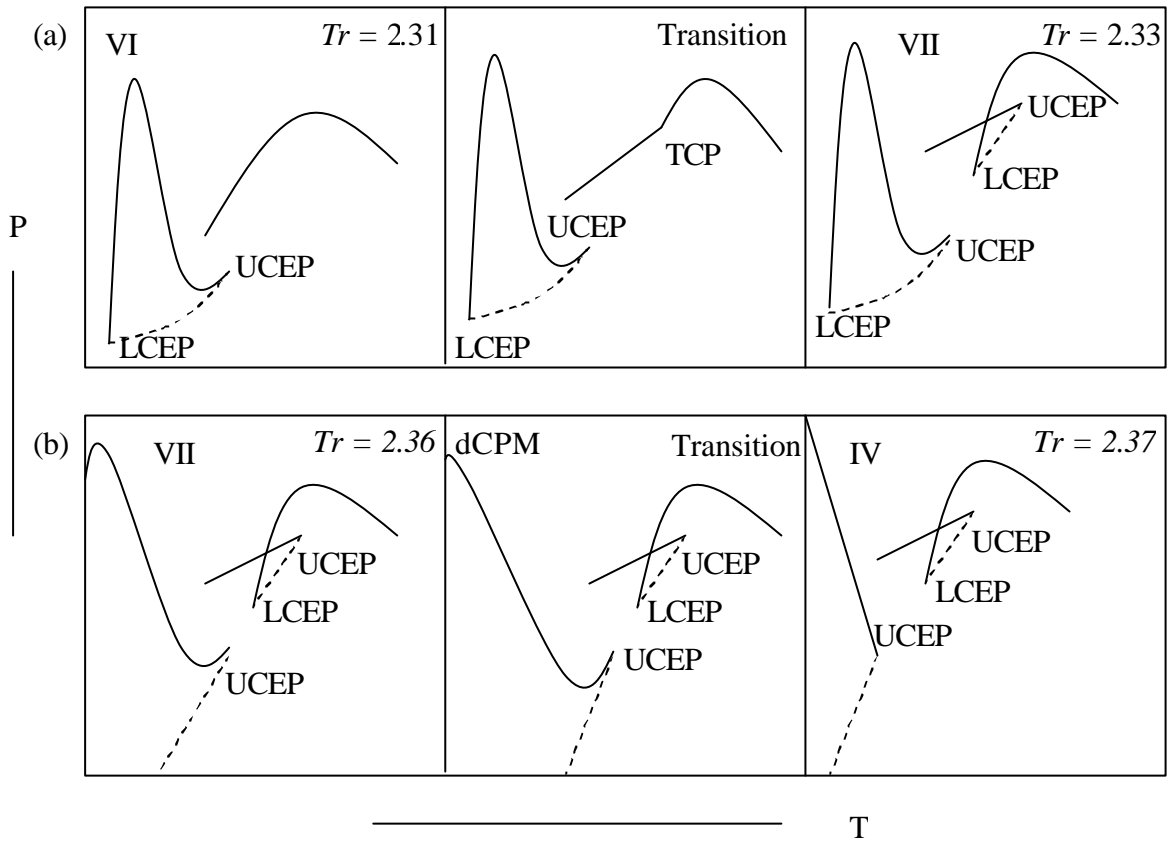


Figure 6.10 The pathway from type VI to type IV in $Vr = 1.7$. Marks (•) are pure critical points. The dashed curves represent LLV curves and the full curves are critical curves.

The observation of type VI and VII behaviour is significant. Previous work that has reported type VI and VII behaviour did so in conjunction with combining rule parameters that represented a significant deviation from the Lorentz-Berthelot combining rules. The results presented here indicate that simply changing the relative values of the critical temperatures and volumes is sufficient to observe type VI and VII behaviour.

6.1.7 Phase Type when $Vr = 1.9$

When $Vr = 1.9$, types I, V, VII, Vm, V and III are found. The pathway of type V to type III is illustrated in the Figure 6.11, and the pathway of type I ? V ? VII ? Vm ? V is illustrated in the Figure 6.12.

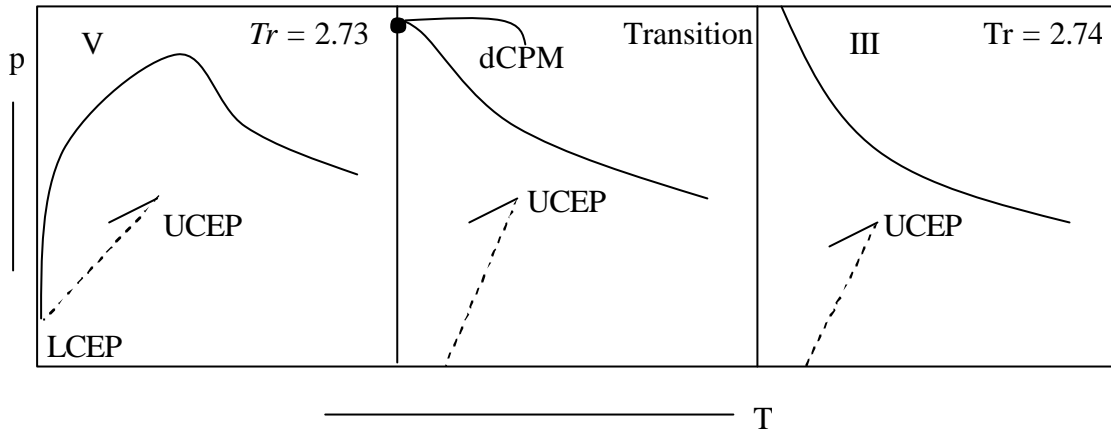


Figure 6.11 The pathway from type V to type III in $Vr = 1.9$. Marks (•) are pure critical points. The dashed curves represent LLV curves and the full curves are critical curves.

The transition diagram of Figure 6.11 is the diagram showing the boundary state (dCPM) of type V and III. Both $Tr = 2.73$ and $Tr = 2.74$ are two calculated points which close to the dCPM boundary. In the Figure 6.12(a), the TCP is shown as boundary between the type I and V; The DCEPs (Figure 6.12(b) and Figure 6.12(c)) are shown as boundary between the V and type VII, and type VII and type Vm; The CPSP (Figure 6.12(d)) is the boundary state of type Vm and type V.

In the diagram of type Vm, the maximum pressure and minimum pressure on the part of the critical curve, which connects with critical point of the pure component with the higher critical temperature merges in a horizontal point of inflection, the CSPPS.

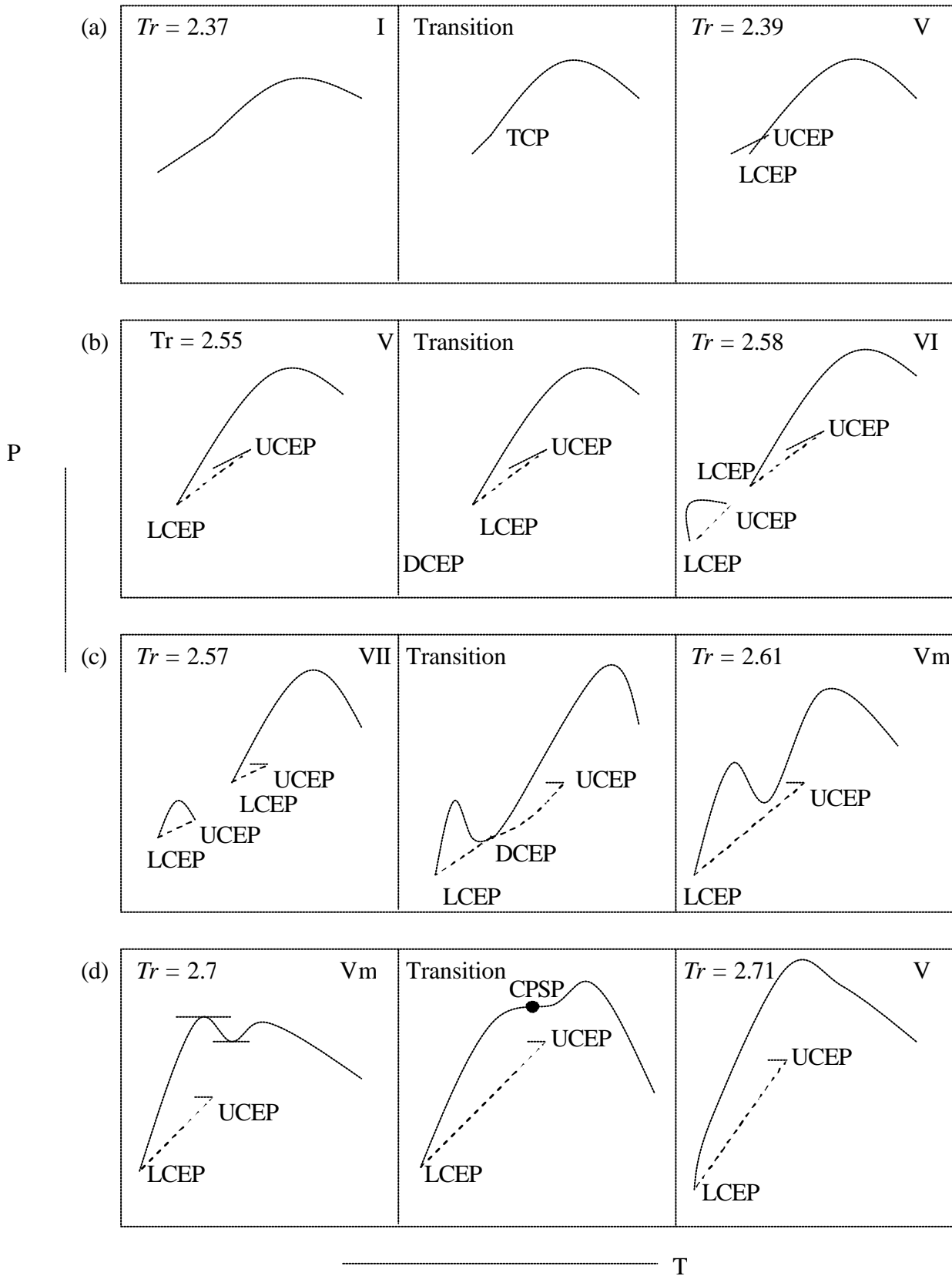


Figure 6.12 The pathway from type I to type V in $Vr = 1.9$. Marks (•) are pure critical points. The dashed curves represent LLV curves and the full curves are critical curves.

6.1.8 Phase Type when $V_r = 2.1$ and over

Type I, V, Vm and III are found when $V_r = 2.1$. Increasing V_r to 2.3, three types I, V and III are obtained when $Tr \geq 1$. For values of $V_r \geq 2.3$, only types I and V are found.

6.1.9 Comparison with Experiment

It is of interest to determine whether this simplified global phase diagram can be used to predict the phase behaviour types of real binary mixtures. To determine this we have identified several binary mixtures of different type. Experimental data for ammonia + alkanes and ammonia + simple gas (Brunner, 1988a), water + noble gases (Wei et al., 1996), methane + n-hexane (Davenport and Rowlinson, 1963) or 1-hexene (Davenport et al., 1966), octadecafluoro-octane + alkanes (Christou et al., 1986), carbon dioxide + hydrocarbon (Sadus and Young, 1985), benzene + alkanes and perfluorobenzene + alkanes (Hicks and Young, 1975; Mainwaring et al., 1987), methanol + alkanes (Brunner, 1985, 1988a; de Loos et al., 1988) and ethane + ethanol and methane + hydrocarbon (ref. van Konynenburg and Scott, 1980) mixtures have been reported. These mixtures and their values of Tr and V_r are summarized in Table 6.1.

These mixtures are located in the global phase diagram (Figure 6.13). Some of these mixtures could not be located in Figure 6.13, because the calculation of the global phase diagram was restricted to $V_r \leq 4$.

In the Table 6.1, the “Yes” means that for this mixtures the experimental type of phase behaviour is located correctly in Figure 6.13, and the “No” means they are not correctly located. The misassignments, are mostly restricted cases of types I/II and type IV/V.

It is significant to note that mixtures of type I, II, III and V behaviour are correctly located on the global phase diagram. However, mixtures of type IV and VI behaviour are not correctly located. This is not surprising because mixtures of these types occur in a very narrow region of the phase diagram and have subtle characteristics. Some binary mixtures such as ammonia + butane, reported as a Type II behaviour (Brunner 1988a), is found in the location of type I in the global phase diagram. It should be noted that the distinction between type I and II mixtures is often hampered by factors such as solidification at very low temperatures. Therefore, in view of such experimental difficulties, the misassignment of type I/II mixture on the global phase diagram is not a serious deficiency. A similar rationale can be used to explain the misassignment of type IV/V mixtures, because the distinction between these systems is an UCST locus which often occurs at low temperatures.

Similarly, some type III systems are located in the type II region of the diagram. However, it can be argued that such impression is relatively small in view of the fact that no attempt has been made to accurately determine the strength of unlike interaction. The extent to which the phase behaviour is misassigned provides an indication of the usefulness of the Lorentz-Berthelot combining rules.

The success of the comparison with experiment means that in many cases, the phase behaviour type of a binary mixture can be predicted based solely on the relative difference in the critical properties of the components. In most cases, the critical properties of the pure components can be used in conjunction with Figure 6.1 to reliably distinguish between types I/II, type III and types IV/V phenomena. In contrast other global phase diagrams rely on the evaluation of unlike interaction parameters (Chapter 4).

Table 6.1 The experimental measure properties of binary mixtures. The symbols (?), (?), (?), (?), (+), (x) and (l) mark the locations of family mixtures in the Figure 6.13.

Mixture	Symbol	Vr	Tr	Type	Is located?	Ref. for Type
Ammonia +	?					Brunner (1988a)
Ethane		2.05	0.75	II	Yes	
Propane		2.82	0.91	II	Yes	
Butane		3.54	1.05	II	No	
Argon		1.04	0.37	III	Yes	
Carbon monoxide		1.29	0.328	III	Yes	
Sulphur hexafluoride		2.75	0.785	III	No	
Methane		1.375	0.47	III	Yes	
Water +	?					Wei et al. (1996)
Helium		1.017	0.008	III	Yes	
Argon		1.34	0.23	III	Yes	
Krypton		1.625	0.323	III	Yes	
Xe		2.1	0.447	III	Yes	
Methane +	l					
n-hexane		3.74	2.67	V	Yes	Davenport and Rowlinson (1963)
3,3-dimethylpentane*		4.18	2.82	IV	No	Van Konynenburg and Scott (1980)
2,3-dimethyl-1-butene		3.46	2.64	IV	No	
2-methyl-1-pentene		3.57	2.66	IV	No	
1-hexene		3.58	2.65	IV	No	Davenport et al. (1966)
Octadecafluoro-octane +	?					Christou et al. (1986)
Hexane		1.35	0.99	II	Yes	
Heptane		1.16	0.93	II	Yes	
Tridecane		1.46	1.347	II	No	
Tetradecane		1.52	1.38	II	No	
Carbon dioxide +	+					Sadus and Young (1985)
Butane		2.71	0.71	II	Yes	
Pentane		3.23	0.65	II	Yes	
Cyclohexane		3.27	0.55	II	No	
Hexane		3.93	0.6	II	Yes	
Methylcyclohexane		3.91	0.53	II	No	
n-tridecane*		8.76	2.22	IV	No	Van der Steen (1989)
Benzene +	?					Mainwaring et al. (1987); Hicks and Young (1975)
Pentane		1.17	0.83	II	Yes	
Hexane		1.43	0.9	II	Yes	
Heptane		1.67	0.96	II	Yes	
Octane		1.9	1.01	II	No	
Nonane		2.12	1.06	II	No	
Decane		2.35	1.09	II	No	
Tridecane		2.7	1.2	II	No	
Perfluorobenzene +	×					Mainwaring et al. (1987)
Pentane		1.06	1.14	II	No	
Hexane		1.14	0.95	II	Yes	
Heptane		1.33	1.01	II	No	
Octane		1.52	1.07	II	No	
Nonane		1.7	1.11	II	No	
Decane		1.91	1.15	II	No	
Dodecane		2.01	1.25	II	No	
Benzene		1.25	0.95	II	Yes	
Cyclohexane		1.05	0.96	II	No	

Table 6.1 continued

Mixture	Symbol	Vr	Tr	Type	Is located?	Ref. for Type
Methanol +	?					
Xenon		1	1.77	II	Yes	Brunner (1985)
Ethane		1.254	0.6	II	Yes	
Propane		1.72	0.72	II	Yes	
Hexane		3.136	0.99	II	Yes	de Loos et al. (1988)
Heptane		3.66	1.055	II	No	
Octane*		4.169	1.109	II	No	
Nonane*		4.661	1.16	II	No	Brunner (1988a)
Decane*		5.288	1.205	II	No	de Loos et al. (1988)
Dodecane*		6.389	1.285	II	No	
Tetradecane*		7.576	1.354	II	No	
Hexadecane*		8.763	1.408	II	No	
Ethane + ethanol		1.69	1.13	V	No	Van Konynenburg and Scott (1980)

* These mixtures occur at outside of the of the Vr - Tr range of Figure 6.13.

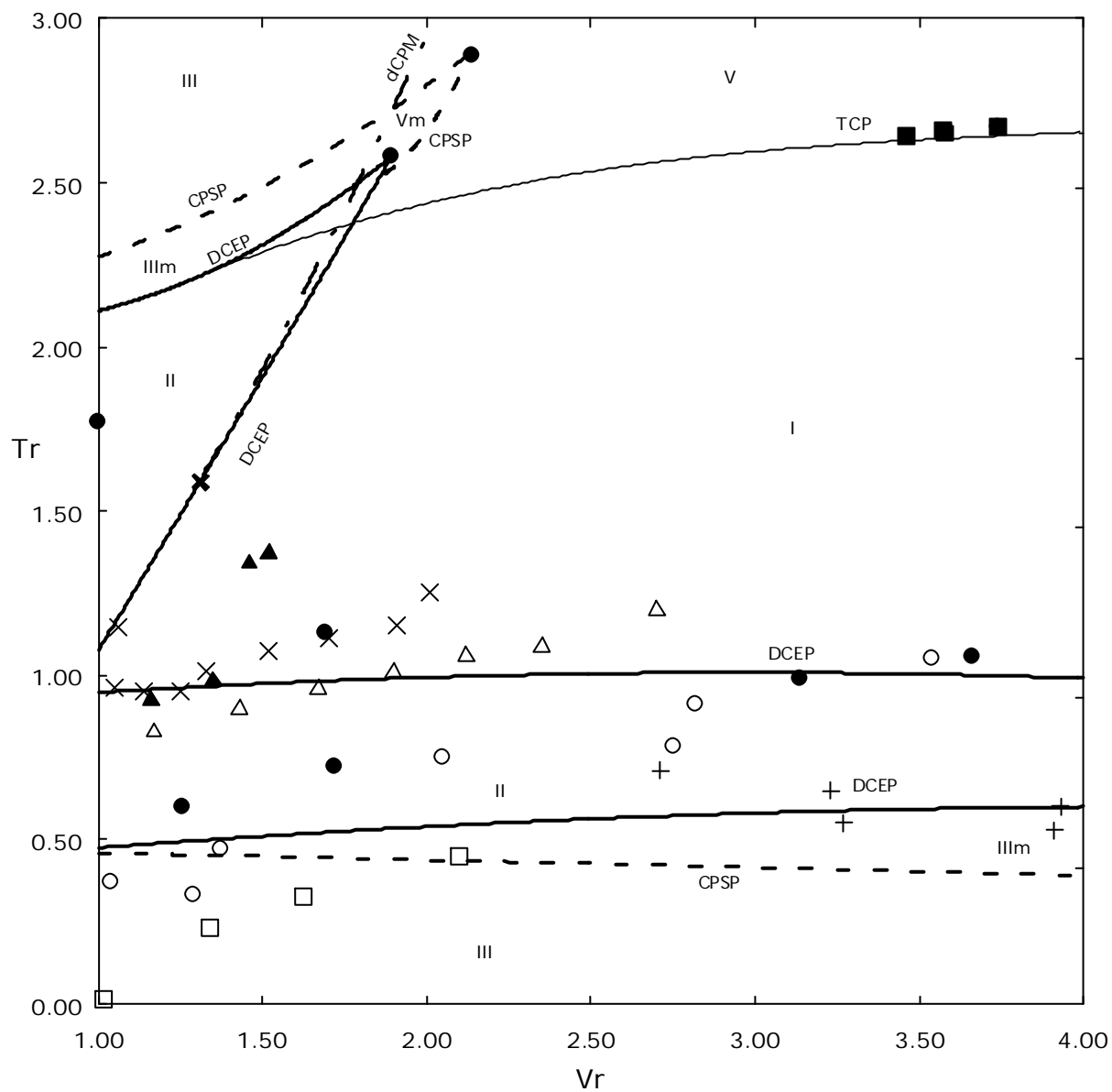


Figure 6.13 The global phase diagram is examined in comparison with experimental binary mixtures. The symbols identifying the different binary mixtures are summarized in Table 6.1.

6.1.10 Comparison with Kolafa's Diagram

Kolafa et al. (1998) have also reported a global phase diagram which is independent of adjustable combining rule parameters. Their diagram was presented as a τ - t projection with

$$t = \frac{a_{22}/\mathbf{s}_{22}^3}{a_{11}/\mathbf{s}_{11}^3} = \frac{T_{22}^C}{T_{11}^C} \quad (6.3)$$

$$l = \frac{\mathbf{s}_{22}}{\mathbf{s}_{11}} = \left(\frac{V_{22}^C}{V_{11}^C} \right)^{1/3} \quad (6.4)$$

where \mathbf{s} is the hard sphere diameter. Kolafa et al. (1998) used the Mansoori-Carnahan-Starling-Leland (MCSL) equation of state (see Eq. 3.74) coupled with the van der Waals attractive term (MCSLvdW) and the original van der Waals equation of state (vdW). For both the CMLvdW and vdW calculations, the one fluid mixing rule (Eq. 3.66) was used for a_m with $a_{12} = \sqrt{a_{11}a_{22}}$. The use of the MCSL equation means that there is no contribution from \mathbf{s}_{12} terms. Similarly, for the vdW calculations, a linear combination for \mathbf{s}_m was used (Eq. 3.65) which means that there is also no contribution from cross terms. Another difference in their calculation is that the Helmholtz function was obtained by directly integrating the equation of state plus an ideal mixing term. In contrast, our calculations used conformal solution theory.

Kolafa et al. were able to identify types I to IV, type VI and type VII phase behaviour. The global phase diagram of Kolafa et al. identified the same boundary states as in the global phase diagram reported here. We have also located these types of behaviour (Figure 6.1 and

6.2). In contrast to Kolafa et al., we were also able to locate type IV behaviour on the global phase diagram (Figure 6.1). This means that the regions of type I/II and type IV/V observed in our global phase diagram are different from those reported by Kolafa et al. (1998). The MCSLvdW and vdW diagrams are qualitatively similar. In both cases the diagrams were obtained without accounting for cross interaction volume terms, i.e., there is no s_{12} and b_{12} term in the MCSLvdW and vdW calculations, respectively. In contrast, our calculations with the CSvdW equation used the one-fluid model to evaluate the contribution from b_{12} . This fact in conjunction with the different model used for the Helmholtz function may explain the differences between the two different global phase diagrams obtained.

Kolafa et al. (1998) did not report a direct comparison of their global phase diagram with experimental data for real binary mixtures.

6.2 Global Phase Diagram for the HCBvdW Equation of State-The Effect of Shape

The understanding and prediction of the phase behaviour of non-spherical molecules is important, most real molecules are neither spherical nor spherically symmetric. To account for the non-spherical geometries of real molecules, Boublik (1981) has reported a theoretically rigorous approach using Kihara's (1963) hard convex body (HCB) concept as an equation of state for hard non-spherical bodies (Eq. 3.43). The HCB concept has been used successfully to predict the properties of simple polyatomic fluids (Svejda and Kohler, 1983; Sadus et al., 1988; Sadus, 1999) and the qualitative behaviour of binary mixtures (Wei and Sadus, 2000).

6.2.1 Calculation Details

We solved the critical conditions of a binary fluid mixture using conformal solution theory (Chapter 2), the one-fluid model (Chapter 2) and the hard convex body van der Waals (HCBvdW) equation of state (Chapter 3). Such theoretically based equations of state have a successful history of correctly predicting the qualitative behaviour of binary mixtures (Wei and Sadus, 2000). The HCBvdW equation allows us to study a hypothetical binary mixture composed of components of identical volume but different geometry as described by the a parameter. A value of $a = 1$ corresponds to a perfect sphere whereas values greater than unity indicate non-spherical geometry. The a of the HCB equation of state has an important influence on the parameter a , which reflects the attractive forces between the molecules, and parameter b which reflects the size of the molecules and the critical compressibility factor Z_c (Chapter 3). In this work, we assume that the size of molecule in binary mixtures are equal, but the molecules have a different shape.

The addition of the shape parameter in the HCBvdW equation of state means that the compressibility factor and equation of state parameters have different values depending on the value of a . At the critical point, the equation of state parameters can be obtained from:

$$b = b^* \frac{RT_c}{p_c} \quad (6.5)$$

$$a = a^* Z_c \frac{R^2 T_c^2}{p_c^2} \quad (6.6)$$

where T_c and p_c are the critical temperature and pressure of mixtures respectively.

In Table 6.2, we summaries the values of a^* , b^* , y_c and Z_c required for the HCBvdW equation of state at different values of a .

Table 6.2 Value of y_c , a^* , b^* and Z_c for the HCBvdW equation of state at different value of a .

a	y_c	Z_c	b^*	a^*
1.0	0.130444	0.3589559	0.1872946	0.49639
2.0	0.089629	0.3528974	0.1265193	0.53583
3.0	0.069295	0.3493835	0.0968421	0.55977
4.0	0.056783	0.3470130	0.0788178	0.57606
5.0	0.048218	0.3452778	0.0665944	0.58793
6.0	0.041953	0.3439524	0.0577193	0.59701
7.0	0.037158	0.3428976	0.0509656	0.60417
8.0	0.033363	0.3420380	0.0456457	0.60999
9.0	0.030282	0.3413140	0.0413427	0.61480
10.0	0.027727	0.3407163	0.0377882	0.61886
20.0	0.015087	0.3375471	0.0203703	0.63978
30.0	0.010377	0.3362892	0.0139587	0.64795
40.0	0.007911	0.3355949	0.0106196	0.65231
50.0	0.006392	0.3351969	0.0085703	0.65502
60.0	0.005363	0.3349004	0.0071843	0.65687
70.0	0.004620	0.3346466	0.0061843	0.65821
80.0	0.004057	0.3345260	0.0054287	0.65923
90.0	0.003617	0.3343700	0.0048377	0.66003
100.0	0.003263	0.3342565	0.0043627	0.66067

6.2.2 Calculations with $a \leq 5$

The binary mixtures reported here represent mixtures of a component of spherical symmetry and a non-spherical component, and the non-spherical molecule has the same volume as the spherical one. Calculations were performed for components with different a ($a = 0.1 \rightarrow 5.0$) and different critical temperature T_r ($T_r = 0.1 \rightarrow 3.0$). This was done to examine the effect of molecular shape in isolation from other influences. For combining rules, we again use Eq. (6.1) and (6.2) without adjustable parameters. The value of a for the mixture was obtained as a linear composition average $a = a_{11}x_{11} + a_{22}x_{11}$. The work of Svejda and Kohler (1983) indicates that this is a reasonable approximation.

The results of the investigation are plotted in a $a-Tr$ projection of the global phase diagram in Figure 6.14. In the absence of other influences the effect of varying a is to generate regions of Types I, II, III and III_m behaviour. We found no evidence of any other phase behaviour type. Only two boundary states were located namely DCEP-double critical end points and CPSP-critical pressure set points. This may indicate that molecular shape as represented by the HCBvdW equation of state plays a relatively minor role on the phase behaviour compared with other influences such as the strength of both like and unlike interaction.

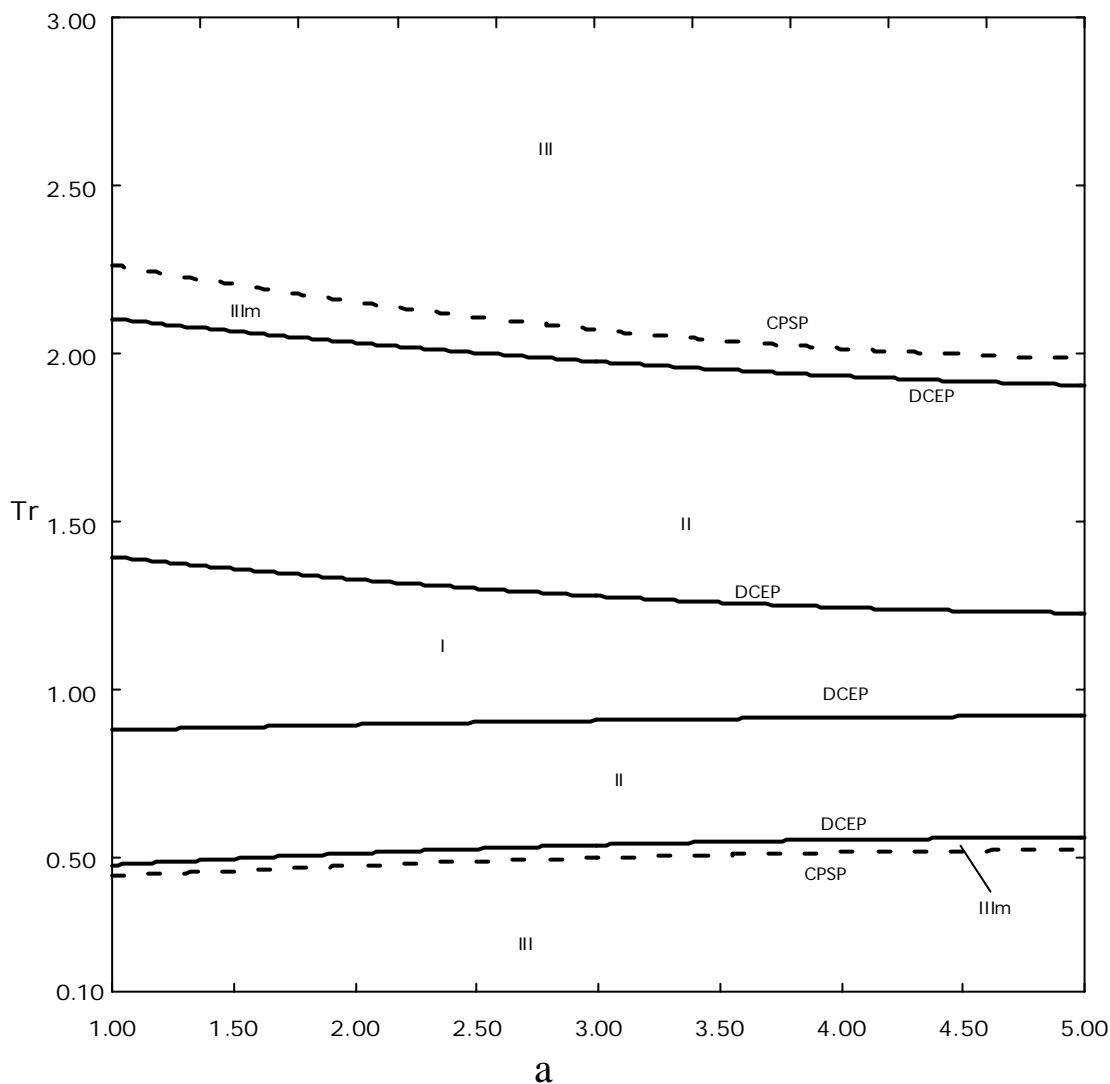


Figure 6.14. Global phase diagram of binary mixtures predicted from HCBvdW equation of state.

6.2.3 Phase Behaviour when $a = 10.0$, 20.0 , and 100.0 .

It is of interest to determine the effect of extreme differences of molecular shape. Figures 6.15 illustrate the pressure-temperature, pressure-mole fraction and pressure-packing fraction ($h = b/4V$, where b is the covolume occupied by the molecules and V is the total volume of the fluid) projection of critical lines in three different mixtures characterized by a second component of different value of a . All data are reported in dimensionless units relative to the corresponding critical property of component 1. Calculations were performed for

components with different critical temperatures. However, the ratio of critical temperatures of component 2 to component 1 illustrated in Figures 6.15 and 6.16 have a constant value of 0.6. In addition to stable lines, metastable lines (extending to negative pressures) are also reported for completeness.

For low values of a (Figure 6.15(a)), type II phenomena are observed with a continuous vapour-liquid critical line linking the pure component critical points, and a separate region of upper critical solution temperature (UCST) extending to high pressures. In contrast to this well-known behaviour, the phenomena observed at higher values of a is different, some part of vapour-liquid critical line are absent. This type behaviour is perhaps a form of type IV behaviour; a three-phase line connects the two branches of the interrupted vapour-liquid critical line, and the UCEP is at the end of the critical line of starting from pure critical point with the highest critical temperature, the LCEP is at the end of the critical line starting from higher temperature pure component critical point. In one sense, it is a “reverse” type IV behaviour because unlike conventional type IV behaviour which the UCEP is connected to the vapour-liquid critical line commencing from the component with the higher not the lower critical temperature.

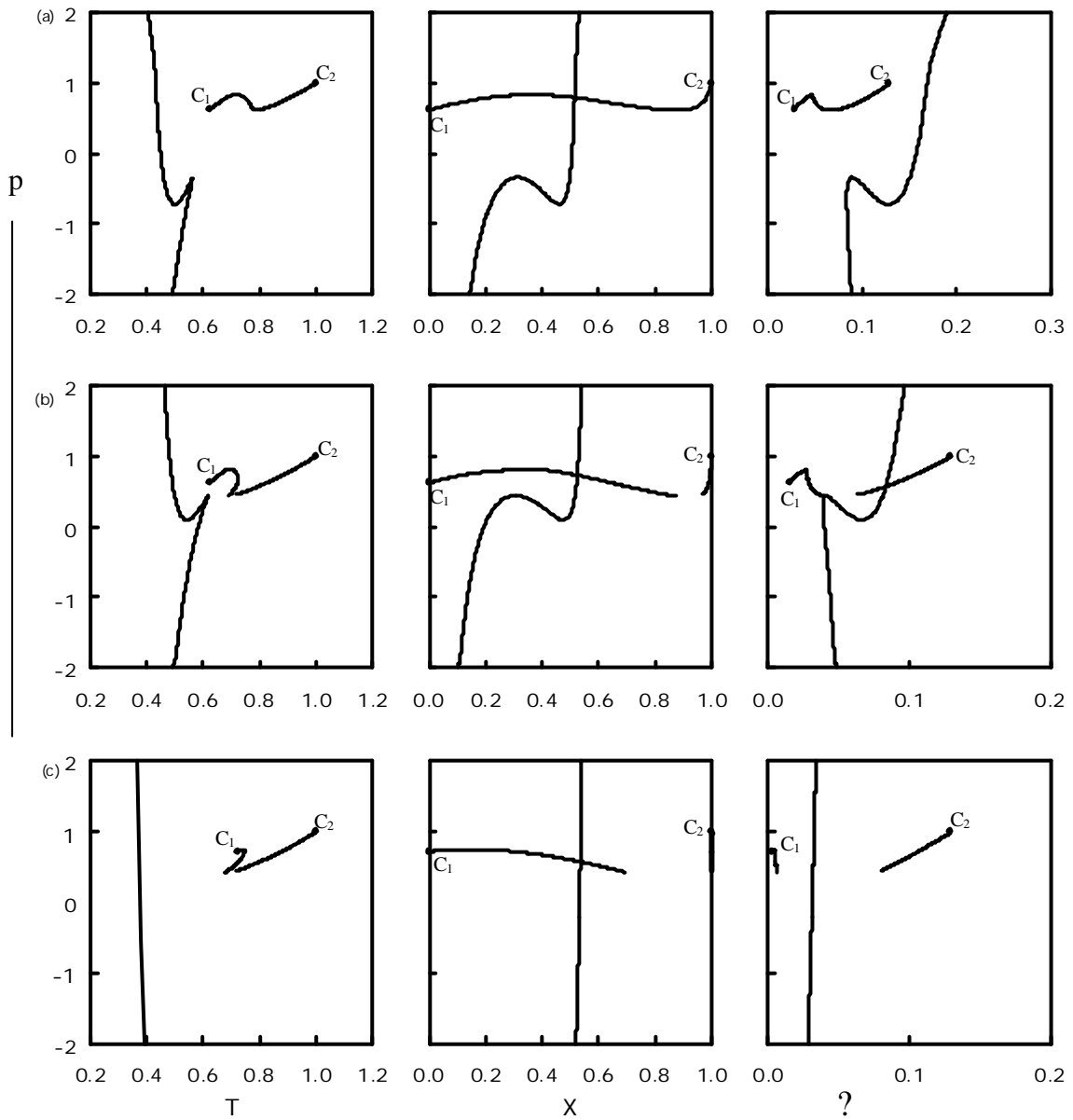


Figure 6.15. The calculated critical properties of a binary at (a) $a = 10.0$, (b) $a = 20.0$, (c) $a = 100.0$ and $Tr = 0.6$

Figure 6.16 is an enlargement of pressure-temperature projection of figure 6.15(b). It shows that critical line which starts from C1 passes through a pressure maximum. By continuing to increase the value of a , the critical curve which connects with the high temperature critical point becomes more contracted (figure 6.15c).

Although the results are for a hypothetical fluid, one can identify certain real types of mixtures for which the phenomena might occur in reality. The requirement of equivalence in molecular volume effectively rules out this phenomenon for mixtures of relatively small molecules because it is unlikely that a small molecule could display the necessary deviation from spherical geometry. Mixtures composed of either a dendrimer or micelle together with either a long chain hydrocarbon or polymer are possible candidate mixtures. The dendrimer/micelle component has a large degree of spherical geometry and the large volume that it occupies could be easily matched by a long chain hydrocarbon/polymer component of highly non-spherical geometry.

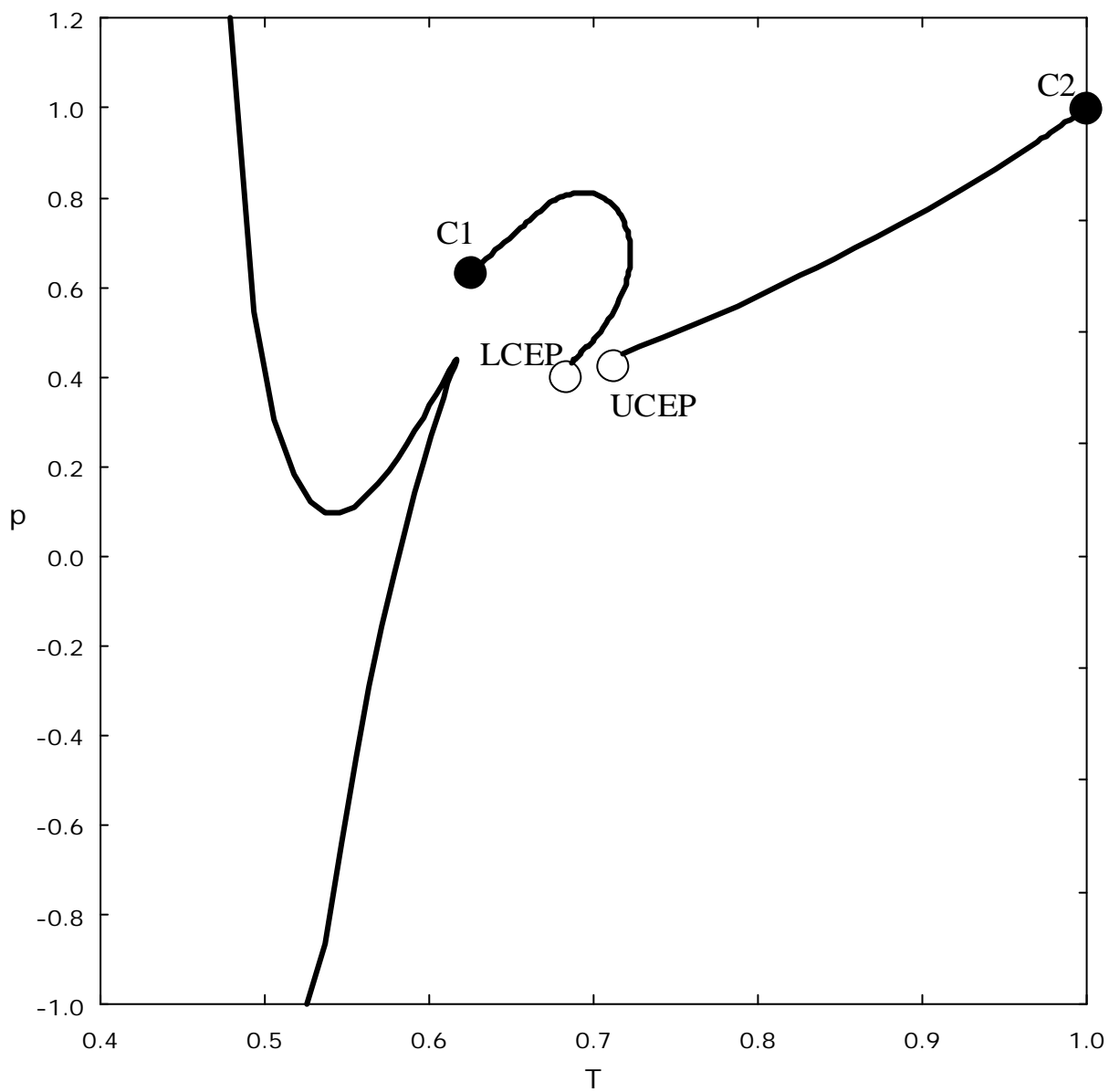


Figure 6.16 Enlargement of figure 6.15(b) of pressure-temperature projection, the marks (?) are pure critical points.

References

- Boublik, T. (1981). Statistical Thermodynamics of Nonspherical Molecule Fluids, *Ber. Bunsenges Phys. Chem.*, **85**, 1038-1041.
- Brunner, E. (1985). Fluid Mixtures at High Pressures II. Phase Separations and Critical Phenomena of (ethane + an n-alkanol) and of (ethane + methanol) and of (propane + methanol), *J. Chem. Thermodynamics*, **17**, 871-885.
- Brunner, E. (1988a). Fluid Mixtures at High Pressures VI. Phase Separations and Critical Phenomena in 18 (n-alkane + ammonia) and 4 (n-alkane + methanol) Mixtures, *J. Chem. Thermodyn.*, **20**, 273-297.
- Brunner, E. (1988b). Fluid Mixtures at High Pressures VII. Phase Separations and Critical Phenomena in 12 Binary Mixtures Containing Ammonia, *J. Chem. Thermodyn.*, **20**, 1379-1409.
- Christou, G., Morrow, T., Sadus, R. J. and Young, C. L. (1986). Phase Behaviour of Fluorocarbon and Hydrocarbon Mixtures: Interpretation of Type II and Type III Behaviour in Terms of a 'Hard-Sphere + Attractive Force' Equation of State, *Fluid Phase Equilib.*, **25**, 263-272.
- Davenport, A. J. and Rowlinson, J. S. (1963). The Solubility of Hydrocarbons in Liquid Methane, *Trans. Faraday Soc.*, **59**, 78-84.
- Davenport, A. J., Rowlinson, J. S. and Saville, G. (1966). Solution of Three Hydrocarbons in Liquid Methane, *Trans. Faraday Soc.*, **62**, 322-327.
- De Loos, T. W, Poot, W. and Swaan Arons, J. (1988). Vapour-Liquid Equilibria and Critical Phenomena in Methanol + N-Alkane Systems, *Fluid Phase Equilib.*, **42**, 209-227.
- Deiters, U. K. and Pegg, I. L. (1989). Systematic Investigation of the Phase Behaviour in Binary Fluid Mixtures, I. Calculations Based on the Redlich-Kwong Equation of State, *J. Chem. Phys.*, **90**, 6632-6641.

- Franck, E. U., Lentz, H. and Welsch, H. (1974). The System Water-Xenon at High Pressures and Temperatures, *Z. Phys. Chem.*, **93**, 95-108.
- Hicks, C. P. and Young C. L. (1975). The Gas-Liquid Critical Properties of Binary Mixtures, *Chem. Rev.*, **75**, 119-175.
- Imre, A. R., Melnichenko, G. and Alexander van Hook, W. (1999). Liquid-Liquid Equilibria in Polystyrene Solutions: the General Pressure Dependence, *Phys. Chem. Chem. Phys.*, **1**, 4287-4292.
- Kihara, T. (1963). Convex Molecules in Gaseous and Crystalline States, *Adv. Chem. Phys.*, **V**, 147-188.
- Kolafa, J., Nezbeda, I., Pavlíček, J. and Smith, W. R. (1998). Global Phase Diagrams of Model and Real Binary Fluid Mixtures: Lorentz-Berthelot Mixture of Attractive Hard Spheres, *Fluid Phase Equilib.*, **146**, 103-121.
- Kolafa, J., Nezbeda, I., Pavlíček, J. and Smith, W. R. (1999). Global Phase Diagrams of Model and Real Binary Fluid Mixtures Part II. Non-Lorentz-Berthelot Mixtures of Attractive Hard Spheres, *Phys. Chem. Chem. Phys.*, **1**, 4233-4240.
- Kraska, T. (1996). Systematic Investigation of the Global Phase Behaviour of Associating Binary Fluid Mixtures: I. Mixtures Containing One Self-Associating Substance, *Ber. Bunsenges Phys. Chem.*, **100**, 1318-1327.
- Kraska, T. and Deiters, U. K., (1992). Systematic Investigation of the Phase Behaviour in Binary Fluid Mixtures. II. Calculations Based on the Carnahan-Starling-Redlich-Kwong Equation of State, *J. Chem. Phys.*, **96**, 539-547.
- Lamm, M. H. and Hall, C. K. (2001). Molecular Simulation of Complete Phase Diagrams for Binary Mixtures, *AIChE J.*, **47**, 1664-1675.
- Lentz, H. and Franck, E. U. (1969). Water-Argon System at High Pressures and Temperatures, *Ber. Bunsenges Phys. Chem.*, **73**, 28-35.

- Mather, A. E., Sadus, R. J. and Franck, E. U. (1993). Phase Equilibria in (Water + Krypton) at Pressures from 31 MPa to 273 MPa and Temperatures from 610K to 660K and in (Water + Neon) from 45 MPa to 255 MPa and from 660K to 700K, *J. Chem. Thermodyn.*, **25**, 771-779.
- Mainwaring, D. E., Sadus, R. J. and Young, C. L. (1987). Deiters' Equation of State and Critical Phenomena, *Chem. Engng. Sci.*, **42**, 459-466.
- Polishuk, I., Wisniak, J., Segura, H., Yelash, L. V. and Kraska, T. (2000). Prediction of the Critical Locus in Binary Mixtures Using Equation of State. II. Investigation of van der Waals-Type and Carnahan-Starling-Type Equation of State, *Fluid Phase Equilib.*, **172**, 1-26.
- Polishuk, I., Wisniak, J. and Segura, H. (2002). Closed Loops of Liquid-Liquid Immiscibility Predicted by Semi-Empirical Cubic Equations of State and Classical Mixing Rules, *Phys. Chem. Chem. Phys.*, **4**, 879-883.
- Rowlinson, J. S. and Swinton, F. L. (1982). Liquids and liquid mixtures, 3rd ed. Butterworths, London.
- Sadus, R. J. (1987). Phase behaviour of binary and tertiary mixtures, PhD Thesis, University of Melbourne.
- Sadus, R. J. and Young, C. L. (1985). Phase Behaviour of Carbon Dioxide and Hydrocarbon Mixing, *Aust. J. Chem.*, **38**, 1739-1743.
- Sadus, R. J., Young, C. L. and Svejda, P. (1988). Application of Hard Convex Body and Hard Sphere Equation of State to the Critical Properties of Binary Mixtures, *Fluid Phase Equilib.*, **39**, 89-99.
- Sadus, R. J. (1999). An Equation of State for Hard Convex Body Chains, *Mol. Phys.*, **97**, 1279-1284.

- Svejda, P. and Kohler, F. (1983). A Generalized van der Waals Equation of State: I. Treatment of Molecular Shape in Terms of the Boublik Nezbeda Equation, *Ber. Bunsenges Phys. Chem.*, **87**, 672-680.
- Tsiklis, D. S. and Prokhorov, V. M. (1966). Mutual Limited Solubility of Gases in the System Water-Argon, *Zh. Fiz. Khim. USSR*, **40**, 2335-2337.
- Van Konynenburg, P. H. and Scott, R. L. (1980). Critical Lines and Phase Equilibria in Binary van der Waals Mixtures, *Philos. Trans. Roy. Soc. London A*, **298**, 495-540.
- Wang, J. L., Wu, G. W. and Sadus, R. J. (2000). Closed-Loop Liquid-Liquid Equilibria and the Global Phase Behaviour of Binary Mixtures Involving Hard-Sphere + van der Waals Interactions, *Mol. Phys.*, **98**, 715-723.
- Wei, Y. S. and Sadus, R. J. (1994). Calculation of the Critical High Pressure Liquid-liquid Phase Equilibria of Binary Mixtures Containing Ammonia: Unlike Interaction Parameters for the Heilig-Franck Equation of State, *Fluid Phase Equilib.*, **101**, 89-99.
- Wei, Y. S. and Sadus, R. J. (1996). Vapour-liquid and Liquid-liquid Phase Equilibria of Binary Mixtures Containing Helium: Comparison of Experiment with Predictions Using Equations of State, *Fluid Phase Equilib.*, **122**, 1-15.
- Wei, Y. S., Sadus, R. J. and Franck, E. U. (1996). Binary Mixtures of Water + Five Noble Gases: Comparison of Binodal and Critical Curves at High Pressures, *Fluid Phase Equilib.*, **123**, 1-15.
- Wei, Y. S. (1998). Prediction of the Fluid Phase Equilibria of Binary and Ternary Mixtures, PhD Thesis, Swinburne University of Technology.
- Wei, Y. S. and Sadus, R. J. (2000). Equations of State for the Calculation of Fluid-Phase Equilibria, *AIChE J.*, **46**, 169-196.
- Wu, G., Heilig, M., Lentz, H. and Franck, E. U. (1990). High Pressure Phase Equilibria of the Water-Argon System, *Ber. Bunsenges Phys. Chem.*, **94**, 24-27.

Yelash, L. V. and Kraska, T. (1998). Closed-Loops of Liquid-Liquid Immiscibility in Binary Mixtures of Equal Sized Molecules Predicted with a Simple Theoretical Equation of State, *Ber. Bunsenges Phys. Chem.*, **102**, 213-223.

Yelash, L. V. and Kraska, T. (1999). The Global Phase Behaviour of Binary Mixtures of Chain Molecules: Theory and Application, *Phys. Chem. Chem. Phys.*, **1**, 4315-4322.